ACS APPLIED MATERIALS & INTERFACES

www.acsami.org

Research Article

High-Toughness and Hierarchical Stress-Dissipating Binder Based on Physicochemical Dual-Cross-Linking for High-Performance Silicon Anodes

Yang He,[§] Feng Zhou,[§] Yingxi Zhang, Tuan Lv, Paul K. Chu, and Kaifu Huo*

Cite This: *ACS Appl. Mater. Interfaces* 2025, 17, 21206−21214

Read Online

ACCESS | Metrics & More | Article Recommendations | Supporting Information

ABSTRACT: Silicon (Si) is a promising anode material for next-generation lithium-ion batteries (LIBs), but the huge volume change of Si particles causes anode fracture and delamination from the current collector, thereby stifling practical implementation. Herein, a high-toughness and hierarchical stress-dissipating binder for Si anodes is prepared by the covalent and hydrogen bonding of poly(acrylic acid) (PAA) and a cross-linked polyurethane (CPU). The physicochemical dual-cross-linked CPU-PAA binder with high toughness, large tensile strength, and hierarchical stress dissipation improves the structural integrity of Si anodes and minimizes thickness swelling. Finite element analysis confirms that the CPU-PAA binder reduces and uniformizes the stress distribution within the Si anodes during cycling. As a result, the Si/CPU-PAA anode shows a high capacity retention of 82.3% after 150 cycles at a high current density of 5 A g^{-1}. Moreover, the Si/CPU-PAA//$LiNi_{0.5}Co_{0.2}Mn_{0.3}O_2$ full cell delivers stable cycling performance, highlighting the great potential of the CPU-PAA binder in high-energy-density LIBs. This work provides insights into the design of high-strength, large-toughness, and efficient stress-dissipating binders for high-performance Si anodes.

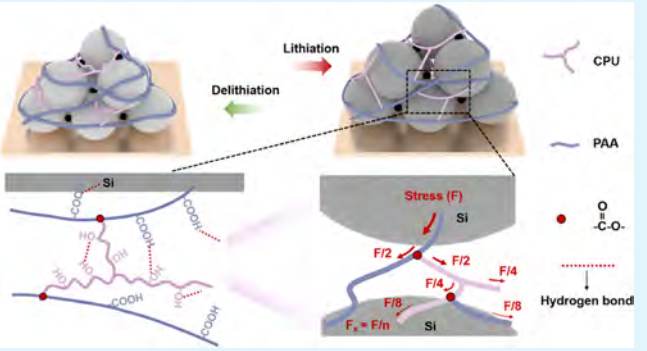

KEYWORDS: *lithium-ion battery, silicon anode, cross-linking binder, hierarchical stress dissipation, high toughness*

1. INTRODUCTION

The rapid development of portable electronics and electric/hybrid vehicles is spurring the demand for lithium-ion batteries (LIBs) with high energy densities.[1,2] Silicon (Si) is a promising anode material for high-energy-density LIBs because of the high theoretical capacity (4200 mAh g^{-1}), which is more than ten times that of graphite (372 mAh g^{-1}).[3,4] However, the large volume change (>300%) of Si during lithiation/delithiation causes materials pulverization, as well as the repeated rupture and reconstruction of the solid electrolyte interface (SEI), further resulting in rapid capacity fading.[5] Nanostructured Si materials, such as nanoparticles and nanowires, can restrain particle pulverization and enhance cycling stability compared to their bulk counterparts.[6−8] However, the repetitive volume expansion and contraction of Si during lithiation/delithiation lead to electrode cracking and delamination, consequently hampering the implementation of Si anodes in high-energy-density LIBs. Developing efficient binders is a feasible strategy to maintain the structural integrity of Si anodes and extend their cycling lifespan.

Binders are important components in anodes as they bind the active materials and conducting agents on the current collector.[9−11] However, the common binders in graphite anodes, such as poly(vinylidene fluoride) (PVDF), are incapable of accommodating the large expansion of Si upon lithiation due to the weak van der Waals force,[12] resulting in detachment of Si particles and poor cycling stability of the battery. The native oxide on Si contains abundant silanol (Si−OH), which can form hydrogen bonds with polar functional groups (e.g., −COOH, −OH, and $-NH_2$).[13−18] Therefore, polymers such as carboxymethyl cellulose (CMC)[19,20] and poly(acrylic acid) (PAA)[21−23] have been proposed as binders for Si anodes. PAA has abundant carboxyl groups,[24] which could form hydrogen bonds with Si−OH groups on the Si surface. Moreover, cross-linked binders based on linear PAA skeleton have been proposed by covalent or physical cross-linking with highly functionalized molecules such as citric acid[25,26] and phytic acid.[27,28] These PAA-based binder networks prevent the sliding of the linear PAA chains, enhancing the adhesion to Si anodes by forming a robust

Received: December 24, 2024
Revised: March 22, 2025
Accepted: March 28, 2025
Published: April 1, 2025

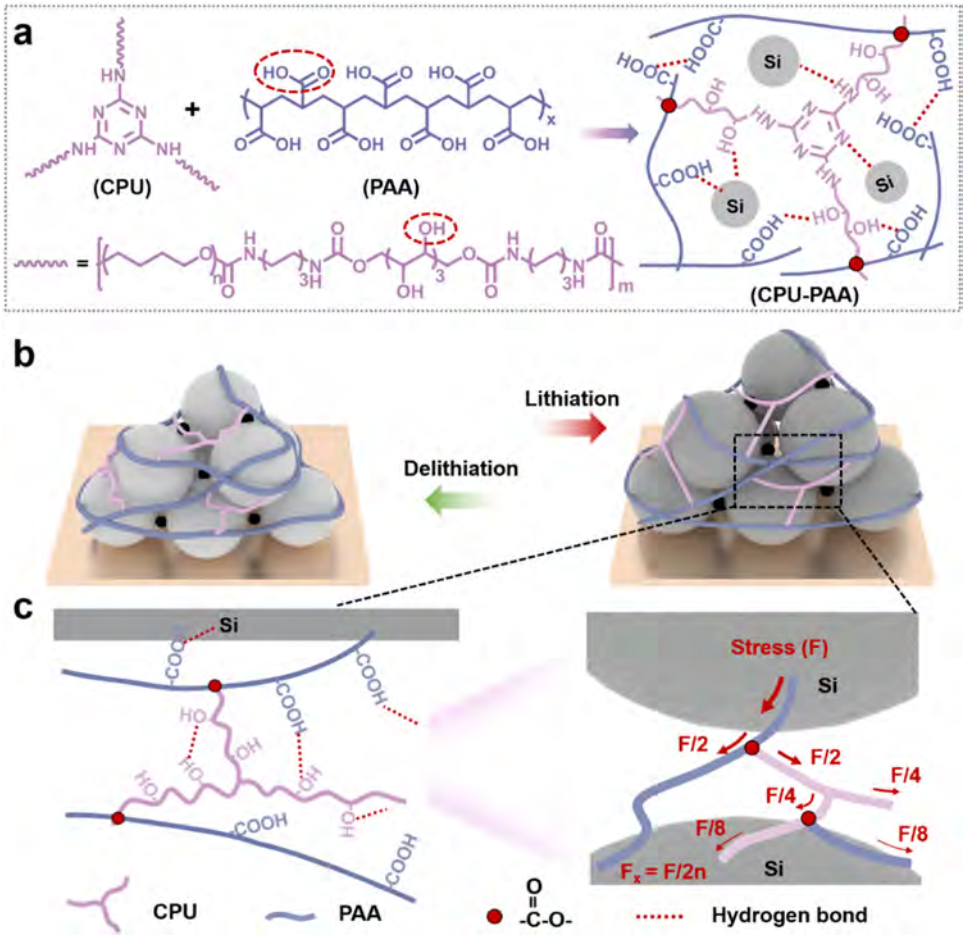

Figure 1. Schematic illustration of the structure of the CPU-PAA binder and Si/CPU-PAA anode. (a) Chemical structure of the CPU-PAA binder and interactions within the Si/CPU-PAA anode. (b) Structural change of the Si/CPU-PAA anode during cycling. (c) Schematic diagram of the hierarchical stress-dissipating network in the Si/CPU-PAA anode.

cross-linked network. However, most of the previously reported PAA-based cross-linked binders display high modulus and poor deformability,[29,30] which are inadequate to address the large volume expansion of Si due to their high mechanical stiffness,[31] especially at high charging/discharging rates. Recently, elastomers containing soft segments, such as carboxyl nitrile rubber (XNBR),[32] styrene−butadiene rubber (SBR),[33] and polyurethane (PU),[34−36] are incorporated into PAA-based binders to balance mechanical strength and toughness.[37] Although elastomers can buffer the volume change of the active Si materials by enhancing elasticity, these binders still suffer from poor and uneven stress dissipation due to insufficient intermolecular interactions between the soft elastomers and rigid PAA chains. The uneven stress dissipation in Si anodes produces a localized stress concentration, which in turn compromises the structural integrity of Si anodes during cycling. Up to now, it is still challenging to produce high-performance binders with high strength, toughness, and efficient stress dissipation for Si anodes.

Herein, a binder boasting high strength, large toughness, and a hierarchical stress-dissipating network is designed for Si anodes by the physicochemical dual-cross-linking of PAA and a cross-linked polyurethane (CPU). The molecular structure and intermolecular interactions of the CPU-PAA binder are depicted in Figure 1a. Specifically, the abundant −OH groups on the three-dimensional (3D) CPU spontaneously form hydrogen bonds with −COOH groups on PAA and Si−OH groups on the Si surface as well as covalent bonds through the in situ esterification reaction. By physicochemically dual-cross-linking the 3D soft CPU segments with the rigid PAA skeleton, the CPU-PAA binder delivers both high strength and toughness and is capable of accommodating the large volume expansion of Si. Moreover, abundant hydrogen bonds and covalently branched chains synergistically assemble a hierarchical stress-dissipating network in the Si/CPU-PAA anode (Figure 1b,c), efficiently distributing and homogenizing expansion stress to maintain the integrity of Si anodes during cycling. Finite element simulation reveals that the average stress in the Si/CPU-PAA anode at the 100% state of charge (SOC) is 72.4% of that in the Si/PAA anode. Consequently, the Si/CPU-PAA anode retains 82.3% of its initial capacity after 150 cycles at a high current density of 5 A g^{-1}, and the Si/CPU-PAA//$LiNi_{0.5}Co_{0.2}Mn_{0.3}O_2$ (NCM) full cell exhibits a high capacity retention of 83.5% after 60 cycles at 0.2 C. The results presented in this work provide insights into the design of high-performance binders for Si anodes.

2. EXPERIMENTAL SECTION

2.1. Materials. Nano silicon powder (Si, 100−200 nm), poly(acrylic acid) (PAA, M_W = 450 000), hexamethylene diisocyanate (HDI), poly(tetrahydrofuran) (PTMEG, M_W ~ 1000), D-glucitol (DG), and adipic acid dihydrazide (ADH)

https://doi.org/10.1021/acsami.4c22696
ACS Appl. Mater. Interfaces 2025, 17, 21206−21214

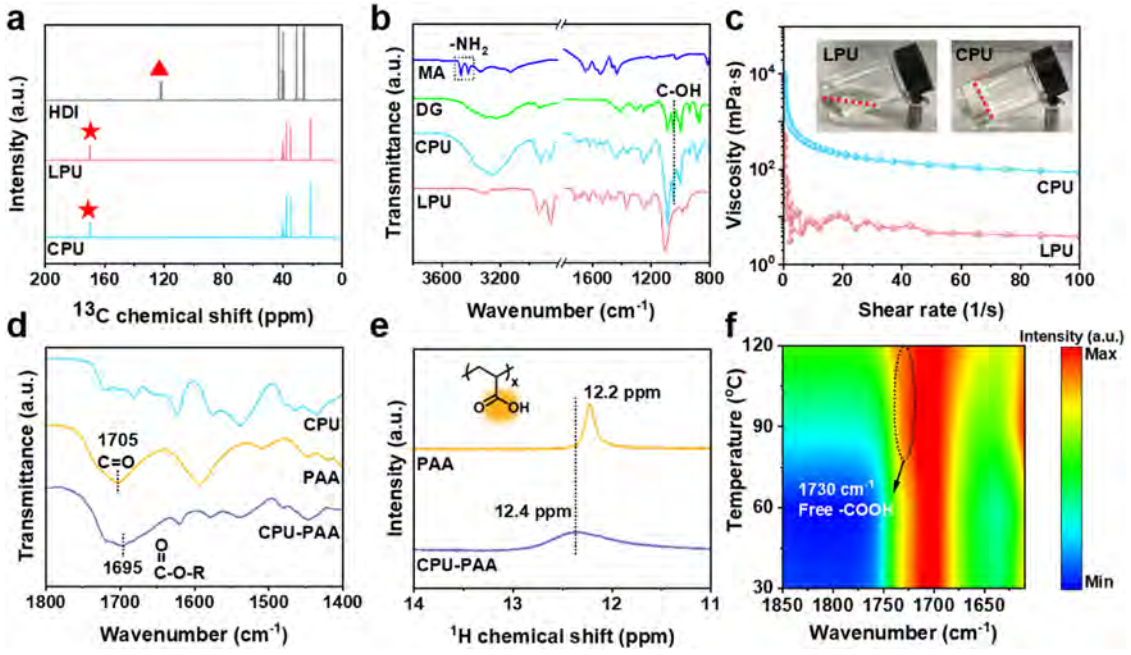

Figure 2. Chemical structure characterization of the polymers. (a) ^{13}C NMR spectra of HDI, LPU, and CPU. (b) ATR-FTIR spectra of MA, DG, LPU, and CPU. (c) Shear viscosity of the LPU and CPU solutions with the insets showing pictures of the solutions. (d) ATR-FTIR spectra of PAA, CPU, and CPU-PAA. (e) ^{1}H NMR spectra of PAA and CPU-PAA. (f) Temperature-dependent ATR-FTIR spectra of CPU-PAA.

are purchased from Shanghai Aladdin Bio-Chsem Technology Co., Ltd. Melamine (MA), ditin butyl dilaurate (DBTDL), and dimethylacetamide (DMAC) are obtained from Sinopharm Chemical Reagent Co., Ltd. All of the reagents are used without further purification.

2.2. Synthesis of CPU and CPU-PAA Binder. PTMEG (0.5 g, 0.5 mmol) and HDI (0.168 g, 1 mmol) are added to DMAC solution and reacted at 80 °C for 3 h under an argon atmosphere. DBTDL (0.01 g, 0.015 mmol) is used as the catalyst. Subsequently, the cross-linker MA (0.0126 g, 0.1 mmol) and chain extender DG (0.0728 g, 0.4 mmol) are introduced into the reaction mixture, and the reaction is continued at 40 °C for 15 h. The product solution is then dried and washed with deionized water to obtain the CPU. In the synthesis of LPU, MA is omitted, and the chain extender ADH (0.087 g, 0.5 mmol) is used in place of DG. All other steps are identical to those in the synthesis of CPU. Subsequently, PAA is dissolved in the above CPU or LPU solution, maintaining a mass ratio of PAA to CPU or LPU at 95:5. The LPU-PAA binder is prepared by drying the mixed solution of LPU and PAA at 80 °C. The CPU-PAA binder is obtained by drying the mixed solution of CPU and PAA at 80 °C, followed by heat treatment at 120 °C for 2 h to facilitate in situ esterification.

2.3. Preparation of Si/CPU-PAA Anodes. Si nanoparticles and Super P are added to a mixed solution of PAA and CPU or LPU, respectively, at a mass ratio of 8:1:1 for Si, binder, and Super P. The slurry is stirred and coated onto the Cu foil, which is fully dried at 80 °C to obtain Si/LPU-PAA anodes. To obtain the Si/CPU-PAA anodes, Si anodes coated with a mixed solution of PAA and CPU are dried at 80 °C and then heat-treated at 120 °C for 2 h. The Si mass loading of the anodes is about 1 mg cm^{-2}.

2.4. Characterization and Measurements. Attenuated total reflectance Fourier transform infrared spectroscopy (ATR-FTIR, Nicolet iS 10 spectrophotometer), scanning electron microscopy (SEM, Hitachi Regulus 8100), nuclear magnetic resonance (NMR, BRUKER AVANCE 400), gel permeation chromatography (GPC, Breeze 2 HPLC system), X-ray photoelectron spectroscopy (XPS), and atomic force microscopy (AFM, Bruker Dimension ICON) are used to analyze the structure and composition of the materials.

2.5. Finite Element Analysis. The finite element analysis is conducted using the COMSOL software by the electrochemical and solid mechanics mode. The key parameters input into the model are listed in the Supporting Information.

3. RESULTS AND DISCUSSION

3.1. Design and Characterization of CPU and CPU-PAA. Figure S1 illustrates the synthesis of the 3D CPU by the condensation reaction of HDI, PTMEG, DG, and MA. For comparison, linear polyurethane (LPU) is synthesized by the condensation reaction of HDI, PTMEG, and ADH without MA and DG (Figure S2). Gel permeation chromatography (GPC) analysis reveals that LPU and CPU have similar molecular weights (Table S1). The chemical structures of CPU, LPU, CPU-PAA, and LPU-PAA are determined by nuclear magnetic resonance (NMR) and attenuated total reflectance Fourier transform infrared (ATR-FTIR) spectroscopy. In the ^{13}C NMR spectra of LPU and CPU, the large peak at 120 ppm corresponding to the isocyanate group (N═C═O) of HDI disappears (Figure 2a), while a new peak at 170 ppm arising from the urethane unit (−NHCOO−) of polyurethane emerges. The ATR-FTIR spectra (Figure 2b) show that the double peaks of $-NH_2$ groups at 3419 and 3469 cm^{-1} in MA vanish in CPU, revealing that the three $-NH_2$ groups in the MA molecule are covalently bonded with the HDI, PTMEG, and DG molecular chains, forming a 3D cross-linked CPU network structure as schematically shown in Figure 1a. Moreover, the introduced DG molecule contains six −OH groups, and the ATR-FTIR spectra of DG and CPU exhibit strong C−OH peaks at 1045 cm^{-1}. The abundant −OH groups along the CPU chains enhance molecular

https://doi.org/10.1021/acsami.4c22696
ACS Appl. Mater. Interfaces 2025, 17, 21206−21214

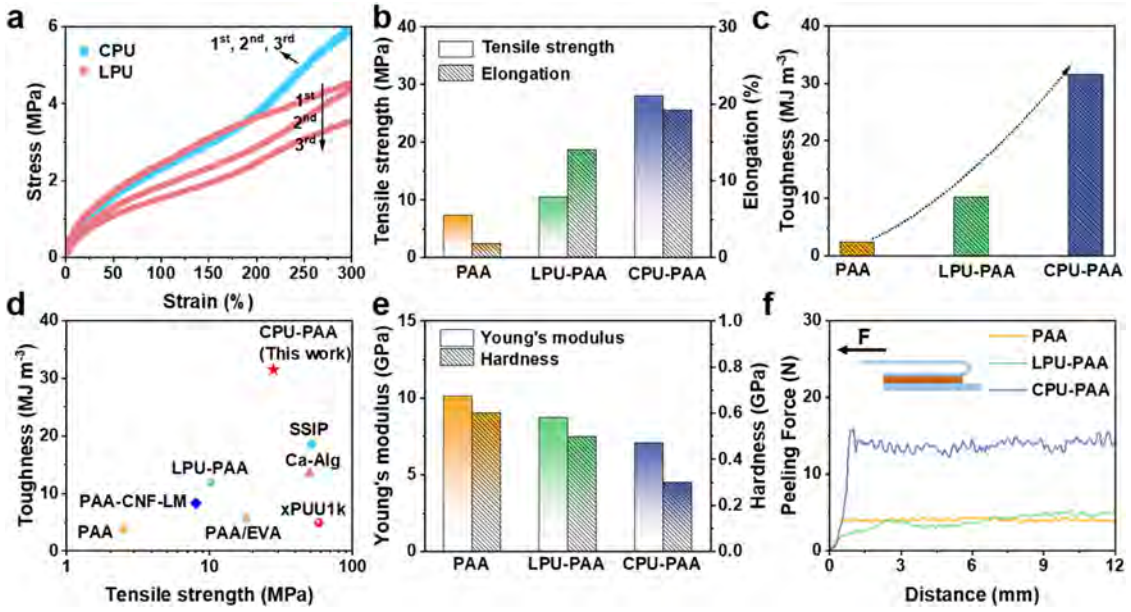

Figure 3. Mechanical properties of the polymers. (a) Stress−strain curves of CPU and LPU from the 1st to 3rd stretching cycles at a fixed elongation of 300%. (b) Comparison of tensile strength and elongation. (c) Comparison of toughness of different binders. (d) Comparison of tensile strength and toughness of binders in this work with binders reported in the literature studies. (e) Comparison of Young's modulus and hardness of different binders. (f) Force−displacement curves of Si anodes with different binders; inset: a schematic of the peeling experiment.

cohesion via interchain hydrogen bonds,[38,39] and therefore, the CPU solution shows much higher viscosity than the LPU solution (Figure 2c).

The CPU-PAA binder is prepared by mixing CPU with PAA, followed by heat treatment at 120 °C for 2 h (Figure S3). The −C═O peak at 1705 cm^{-1} of PAA red shifts to 1695 cm^{-1} in CPU-PAA (Figures 2d and S4), indicating that the −OH groups of CPU form covalent ester linkages with the −COOH groups of PAA. The ^1H NMR spectrum in Figure 2e reveals the downfield shift of the proton peak of −COOH from 12.2 ppm for PAA to 12.4 ppm for CPU-PAA. Moreover, the peak is broadened due to the deshielding effect of interchain hydrogen bonds,[40,41] suggesting the formation of abundant hydrogen bonds between PAA and CPU. The temperature-dependent ATR-FTIR spectra (Figure 2f) show that the peak at 1730 cm^{-1} for free −COOH groups gradually intensifies with temperature due to the disassociation of hydrogen bonds, further confirming the presence of abundant hydrogen bonding in CPU-PAA.[42] The 3D soft CPU segments and rigid PAA skeleton are physicochemical dual-cross-linked by hydrogen bonds and covalent ester linkages in CPU-PAA. Therefore, the CPU-PAA binder is expected to have high strength, large toughness, and a hierarchical stress-dissipating network. In contrast, the soft LPU segments and rigid PAA chains in the LPU-PAA binder are physically mixed without cross-linking (Figure S5), resulting in poor toughness and stress-dissipating properties.

3.2. Mechanical Properties of CPU and CPU-PAA. Tensile tests are conducted to evaluate the mechanical properties of CPU, LPU, CPU-PAA, and LPU-PAA polymers. As shown in Figure S6, CPU has excellent mechanical strength (14.1 MPa) and elongation (2340%), which are significantly higher than those of LPU (7.2 MPa and 536%). During repeated stretching with a fixed elongation of 300% and relaxation time of 30 min, the stress in LPU at a given strain decreases progressively from the first to the third stretching cycle. However, the three stress−strain curves of CPU nearly overlap (Figure 3a), demonstrating the excellent mechanical dissipation and resilience of CPU.[43] The improved tensile strength, elongation, and resilience of CPU over LPU are primarily attributed to the robust 3D structure formed by integrating the three linear soft segments with the MA cross-linker.

CPU is further physicochemically dual-cross-linked with PAA to form the CPU-PAA binder with exceptional tensile strength of 28.0 MPa and elongation of 19.2% (Figure 3b), surpassing those of the LPU-PAA (10.5 MPa and 14.0%), PAA (7.4 MPa and 1.8%), and previously reported binders (Figure S7−S8). Based on the stress−strain curves in Figure S9, the CPU-PAA binder has a calculated toughness of up to 31.5 MJ m^{-3} (Figure 3c), which is better than those of LPU-PAA (10.2 MJ m^{-3}) and PAA binders (2.5 MJ m^{-3}). Figure 3d and Table S2 compare the toughness and tensile strength of CPU-PAA with those of other reported binders, revealing that the CPU-PAA binder has the highest toughness and offers the optimal balance between toughness and tensile strength. Moreover, the CPU-PAA binder has the lowest Young's modulus and hardness (7.0 and 0.3 MPa) compared to the LPU-PAA (8.7 and 0.5 MPa) and PAA binders (10.1 and 0.6 MPa), as shown in Figures 3e and S10. The CPU-PAA binder combines the mechanical advantages of 3D soft CPU and rigid PAA skeleton through physicochemical dual-cross-linking, effectively meeting the binder requirements for Si anodes during cycling and maintaining their structural integrity.

The adhesion strengths of Si/CPU-PAA, Si/LPU-PAA, and Si/PAA to the Cu current collector are evaluated by 180° peeling experiments, as shown in the inset of Figure 3f. The Si/CPU-PAA anode demonstrates an average peeling force of 13.7 N, which is higher than those of the Si/PAA (4.0 N) and Si/LPU-PAA (4.2 N) anodes. The improved interfacial adhesion of the Si/CPU-PAA anode to the Cu foil stems from the enhanced interactions between Si particles, Cu interface, and 3D CPU-PAA chains due to abundant 3D

https://doi.org/10.1021/acsami.4c22696
ACS Appl. Mater. Interfaces 2025, 17, 21206−21214

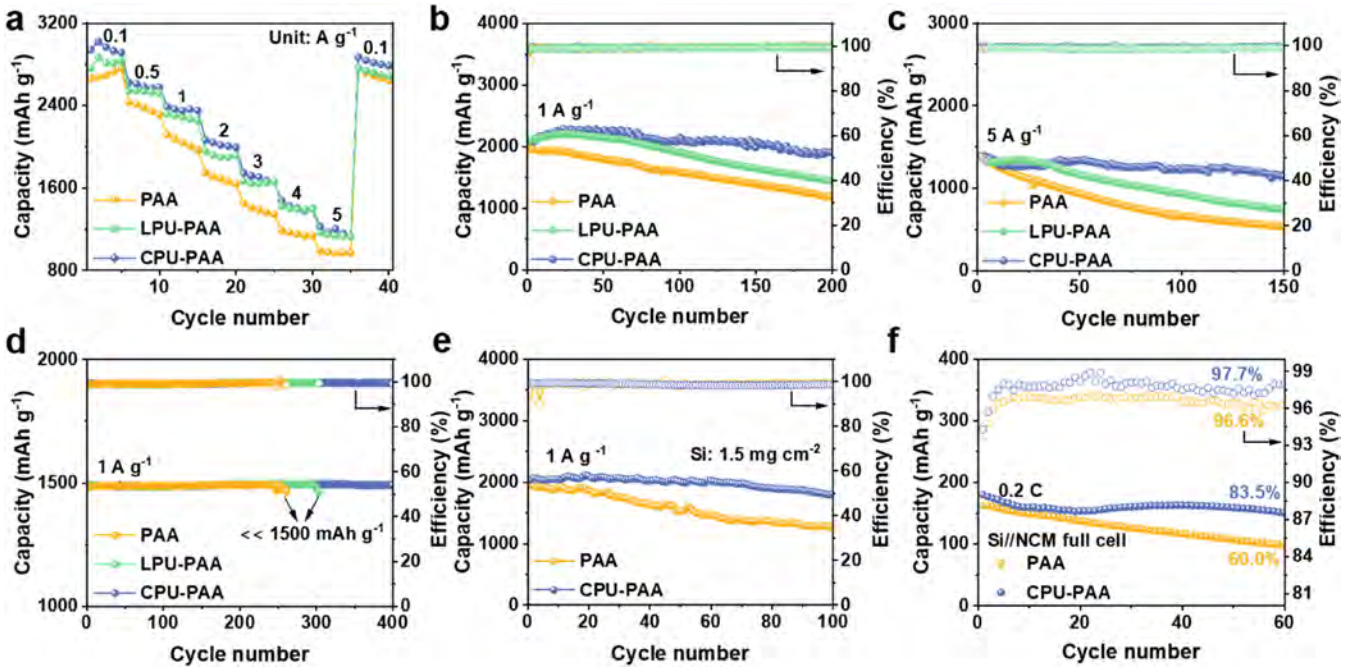

Figure 4. Electrochemical properties of the Si anodes with the PAA, LPU-PAA, and CPU-PAA binders in Si//Li half-cells and NCM//Si full cells. (a) Rate performance of the Si anodes (Si mass loading ≈ 1 mg cm^{-2}) in half-cells. Cycling characteristics of the Si anodes (Si mass loading ≈ 1 mg cm^{-2}) in half-cells at (b) 1 A g^{-1}, (c) 5 A g^{-1}, and (d) 1 A g^{-1} with a fixed capacity of 1500 mAh g^{-1}. (e) Cycling characteristics of the Si anodes in half-cells at 1 A g^{-1} with a high Si mass loading of 1.5 mg cm^{-2}. (f) Cycling characteristics of the Si/CPU-PAA and Si/PAA anodes (Si mass loading ≈ 1.5 mg cm^{-2}) in NCM//Si full cells at 0.2 C.

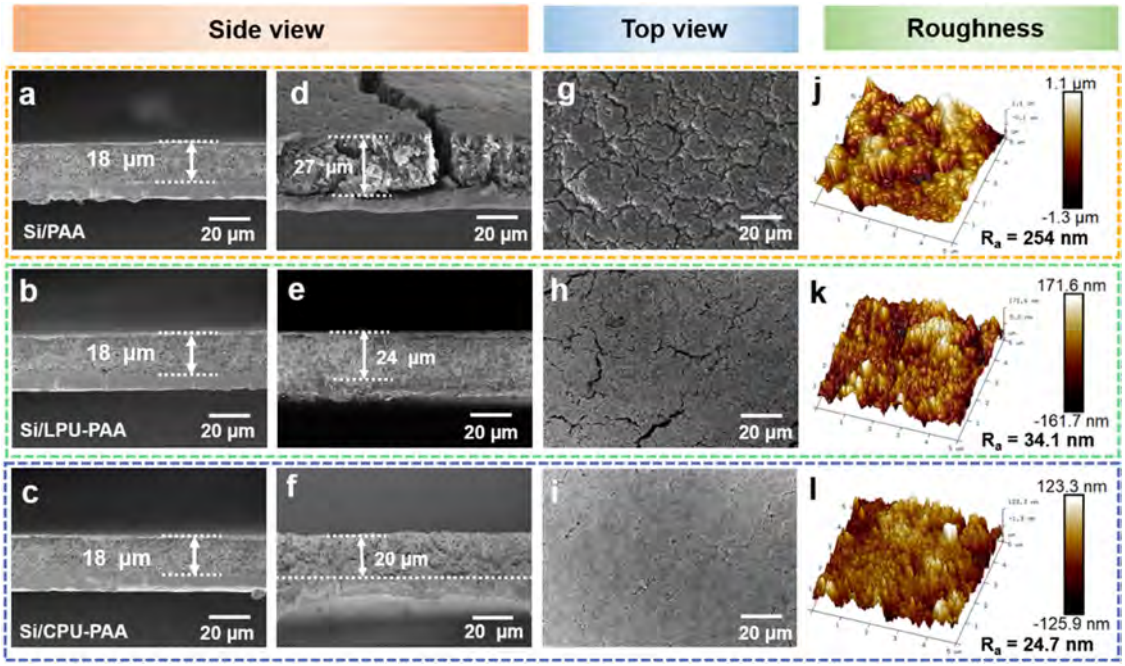

Figure 5. Morphology of the Si/PAA, Si/LPU-PAA, and Si/CPU-PAA anodes before and after 50 cycles in Si//Li half-cells. (a–c) Side-view SEM images of different Si anodes before cycling. (d–f) Side-view SEM images of different Si anodes after cycling. (g–i) Top-view SEM images of different Si anodes after cycling. (j–l) 3D AFM images of different Si anodes after cycling.

hydrogen bonding, which is crucial to mitigate the delamination of active materials from the Cu current collector.

3.3. Electrochemical Characteristics. The electrochemical stability of the binders is evaluated by linear sweep voltammograms (LSV) and cyclic voltammetry (CV).[44,45] As shown in Figure S11, no oxidation or reduction peaks associated with PAA, LPU-PAA, and CPU-PAA are observed between 0.01 and 4.6 V, indicating excellent electrochemical stability in a wide electrochemical window. The CV curves of Si/PAA, Si/LPU-PAA, and Si/CPU-PAA anodes exhibit similar shape. The reduction peak around 0.2 V is ascribed to the transformation of Si to Li_xSi, while the oxidation peaks at 0.3 and 0.5 V correspond to the two dealloying processes of Li_xSi to Si (Figure S12).

https://doi.org/10.1021/acsami.4c22696
ACS Appl. Mater. Interfaces 2025, 17, 21206–21214

Figure 4a depicts the rate performance of Si/PAA, Si/LPU-PAA, and Si/CPU-PAA anodes in Si//Li half-cells from 0.01 to 1.0 V, and the related charge−discharge voltage curves are presented in Figure S13. The Si/CPU-PAA anode exhibits specific capacities of 2956, 2592, 2364, 2025, 1700, 1418, and 1177 mAh g^{-1} at 0.1, 0.5, 1, 2, 3, 4, and 5 A g^{-1}, respectively, which are higher than those of the Si/LPU-PAA and Si/PAA anodes. In long-term operation, the Si/CPU-PAA anode shows a specific capacity of 1903 mAh g^{-1} and a capacity retention of 83.2% after 200 cycles at 1 A g^{-1} (Figure 4b), surpassing the Si/LPU-PAA (65.4%) and Si/PAA (59.6%) anodes. Even at a high current density of 5 A g^{-1} (Figure 4c), the Si/CPU-PAA anode retains 82.3% of the capacity after 150 cycles, which significantly outperforms the Si/LPU-PAA anode (53.5%), Si/PAA anode (38.4%), as well as previously reported Si anodes (Figure S14). Figure 4d depicts the cycling stability of the Si anodes with a fixed specific capacity of 1500 mAh g^{-1} at 1 A g^{-1}. The Si/CPU-PAA anode shows a lifespan of 400 cycles, whereas the Si/LPU-PAA and Si/PAA anodes exhibit significant capacity degradation before 300 and 250 cycles, respectively. Remarkably, the Si/CPU-PAA anode maintains high capacity retention of 88.5% and 83.3% after 100 cycles at Si mass loadings of up to 1.5 and 2.1 mg cm^{-2}, respectively (Figures 4e and S15), significantly outperforming the Si/PAA anodes, which show a capacity retention of 65.0 and 63.6%, respectively. The hierarchical stress-dissipating binder network with high toughness in the Si/CPU-PAA anodes effectively reduces stress distribution and enhances structural integrity, thereby enabling enhanced electrochemical performance.

The practicability of the CPU-PAA binder is explored using full cells assembled with the Si/CPU-PAA, Si/PAA anodes, and NCM cathodes. After 60 cycles at 0.2 C (Figure 4f), the Si/CPU-PAA//NCM full cell shows higher capacity retention of 83.5% than the Si/PAA//NCM full cell (60.0%). Additionally, the Si/CPU-PAA//NCM full cell achieves an average Coulombic efficiency of 97.7%, which surpasses 96.6% for the Si/PAA//NCM full cell. The results further confirm the great potential of the CPU-PAA binder for Si anodes in high-energy-density LIBs.

3.4. Electrode Morphology Characterization. In order to determine the influence of the binders on the structural changes of Si anodes, scanning electron microscopy (SEM) is used to observe the morphology before and after 50 cycles. The thickness fluctuations of the anodes are visualized using cross-sectional SEM images. Figure 5a−c shows that the initial thicknesses of the Si/PAA, Si/LPU-PAA, and Si/CPU-PAA anodes are about 18 μm with Si mass loading of 1 mg cm^{-2}. After 50 cycles, the thicknesses of the Si/PAA and Si/LPU-PAA anodes increase to 27 and 24 μm (Figure 5d,f), corresponding to swelling ratios of 50.0 and 33.3%. However, the thickness of the Si/CPU-PAA anode increases slightly to 20 μm, exhibiting a low swelling ratio of 11.1%. Figures 5d,g, and S16 reveal that the Si/PAA anodes fracture after 50 cycles due to the poor toughness and sliding of linear PAA molecular chains. Although LPU-PAA enhances the toughness and restrains the detachment of the Si/LPU-PAA anode and the cross section of the Si/LPU-PAA anode is relatively integrated, the top-view SEM image in Figure 5h reveals the presence of many cracks in the Si/LPU-PAA anodes. In contrast, the top-view and cross-sectional SEM images of the Si/CPU-PAA anode after 50 cycles show a crack-free and smooth morphology (Figure 5f,i), which is very similar to the Si/CPU-PAA anode before cycling (Figure S17).

The surface morphological changes of the Si/PAA, Si/LPU-PAA, and Si/CPU-PAA anodes are also investigated by atomic force microscopy (AFM), as shown in Figure 5j−l. Before cycling, the anode surface is smooth with an average surface roughness of nearly 25 nm (Figure S18). However, the surface roughness of the Si/PAA anode increases dramatically to 254.0 nm after 50 cycles due to cracking. In comparison, the roughness of the Si/LPU-PAA anode increases to 34.1 nm, and that of the Si/CPU-PAA anode remains almost unchanged (24.7 nm), further confirming the superiority of the physicochemical dual-cross-linked CPU-PAA binder for structural integrity.

The electrochemical impedance spectroscopy (EIS) of Si/PAA, Si/LPU-PAA, and Si/CPU-PAA electrodes before and after 200 cycles is shown in Figure S19 and Table S3. The Si/PAA, Si/LPU-PAA, and Si/CPU-PAA electrodes have similar values of charge transfer resistance (R_{ct}) before cycling. However, the R_{ct} values of the Si/PAA and Si/LPU-PAA electrodes increase significantly to 148.3 and 119.4 Ω after 200 cycles. By contrast, the R_{ct} of the Si/CPU-PAA electrode increases slightly to 85.2 Ω after 200 cycles, suggesting more efficient charge transfer enabled by the CPU-PAA binder due to the enhanced toughness and stress dissipation performance. After cycling, the strong LiF signal peak in the XPS spectra indicates a LiF-rich layer on the surface of Si/CPU-PAA electrode (Figure S20).[46]

3.5. Finite Element Simulation. Finite element analysis is performed to study the stress evolution and distribution in the Si/PAA and Si/CPU-PAA anodes at different SOC.[47] A 3D geometric model with spherical Si particles randomly distributed in the binder matrix is constructed using the COMSOL software (Figure 6a−c), and the relevant parameters are depicted in Table S4.

During the lithiation process, Si particles are lithiated to form $Li_{15}Si_4$, and the huge volume change causes a large expansion stress in the Si/PAA and Si/CPU-PAA anodes. Figure 6d,e depicts the cross-sectional views of the stress distributions in the Si/PAA and Si/CPU-PAA anodes at different SOC. The results show that expansion stress is locally concentrated within the Si/PAA anodes. However, the stress concentration in the Si/CPU-PAA anode is significantly relieved. Figure 6f shows the average stress in the Si/CPU-PAA and Si/PAA anodes during lithiation. In 100% SOC, the average stress of the Si/CPU-PAA anode is 108.0 MPa, which is much lower than the 149.1 MPa of the Si/PAA anode. The simulation results are derived from our experimental data (Figure S21a) and the theoretical work of Cui's group[48] (Figure S21b), which show a strong correlation with the experimental results on electrode volume expansion and cracking.

4. CONCLUSIONS

A novel physicochemical dual-cross-linked binder is designed and fabricated for Si anodes via the covalent and hydrogen bonding of 3D soft CPU segments and rigid PAA skeleton. The physicochemical dual-cross-linked binder exhibits high toughness, large tensile strength, large antipeeling capability, and low Young's modulus, enhancing the structural integrity of Si anodes during cycling and minimizing anode swelling. Finite element analysis reveals that the CPU-PAA binder reduces and uniformizes the stress distribution of the Si anode during lithiation, giving rise to a low average stress in the Si/CPU-PAA anode, which is 72.4% of that in the Si/PAA anode.

https://doi.org/10.1021/acsami.4c22696
ACS Appl. Mater. Interfaces 2025, 17, 21206−21214

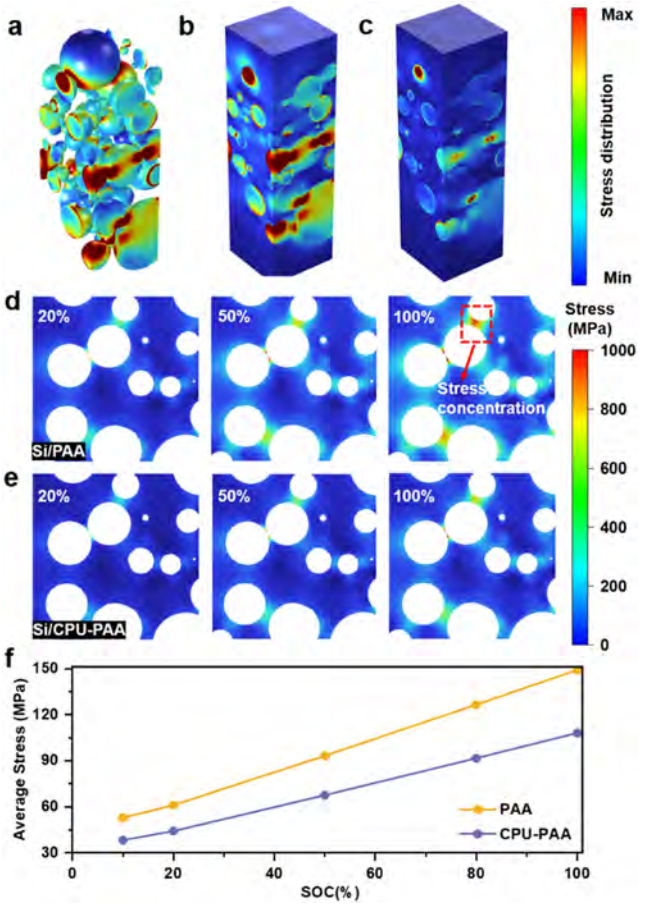

Figure 6. Structure and stress evolution of Si anodes during lithiation by finite element analysis. Stress distributions of (a) Si particles, (b) Si/PAA anodes, and (c) Si/CPU-PAA anodes during lithiation. Cross-sectional views of the stress distributions of (d) Si/PAA and (e) Si/CPU-PAA anodes at different SOC. (f) Comparison of the average stress in the Si/PAA and Si/CPU-PAA anodes at different SOC.

Owing to these merits, the Si/CPU-PAA anode exhibits a high capacity retention of 82.3% after 150 cycles at a large current density of 5 A g^{-1}. Moreover, the Si/CPU-PAA//NCM full cell shows a low-capacity decay of 0.27% per cycle at 0.2 C. The enhanced cycling stability results from the physicochemical dual-cross-linked CPU-PAA binder, which combines the advantages of the 3D soft CPU segments with the rigid PAA skeleton and further forms an efficient hierarchical stress-dissipating network in the Si/CPU-PAA anodes. The results provide novel insights into the development of high-performance binders for Si anodes in high-energy-density LIBs.

■ ASSOCIATED CONTENT

Supporting Information

The Supporting Information is available free of charge at https://pubs.acs.org/doi/10.1021/acsami.4c22696.

Synthesis and chemical structure of CPU and CPU-PAA; ATR-FTIR spectra of CPU-PAA; stress−strain curves of LPU and CPU, LPU-PAA, and CPU-PAA; LSV curves of PAA, LPU-PAA, and CPU-PAA; comparison of the stress and strain of the CPU-PAA binder and binders in literature studies; CV curves of Si/PAA//Li, Si/LPU-PAA//Li, and Si/CPU-PAA//Li half-cells; comparison of the capacity retention of the Si electrode with the CPU-PAA binder with those of similar binders in the literature; initial morphology of the Si electrode at different magnifications; and AFM images of the pristine Si electrode (PDF)

■ AUTHOR INFORMATION

Corresponding Author

Kaifu Huo − *Wuhan National Laboratory for Optoelectronics (WNLO), Huazhong University of Science and Technology, Wuhan 430074, P. R. China;* orcid.org/0000-0001-5670-8233; Email: kfhuo@hust.edu.cn

Authors

Yang He − *Wuhan National Laboratory for Optoelectronics (WNLO), Huazhong University of Science and Technology, Wuhan 430074, P. R. China*

Feng Zhou − *Wuhan National Laboratory for Optoelectronics (WNLO), Huazhong University of Science and Technology, Wuhan 430074, P. R. China;* orcid.org/0000-0003-3548-735X

Yingxi Zhang − *Wuhan National Laboratory for Optoelectronics (WNLO), Huazhong University of Science and Technology, Wuhan 430074, P. R. China; Department of Physics, Department of Materials Science and Engineering, and Department of Biomedical Engineering, City University of Hong Kong, Kowloon, Hong Kong 999077, P. R. China*

Tuan Lv − *Wuhan National Laboratory for Optoelectronics (WNLO), Huazhong University of Science and Technology, Wuhan 430074, P. R. China*

Paul K. Chu − *Department of Physics, Department of Materials Science and Engineering, and Department of Biomedical Engineering, City University of Hong Kong, Kowloon, Hong Kong 999077, P. R. China;* orcid.org/0000-0002-5581-4883

Complete contact information is available at: https://pubs.acs.org/10.1021/acsami.4c22696

Author Contributions

[§]Y.H. and F.Z. contributed equally to this work. K.H. conceived the idea. Y.H. designed the experiments and wrote the draft. Y.H., F.Z., Y.Z., and T.L. carried out material fabrication and characterization. Y.H. and F.Z. performed electrochemical test and property characterizations. F.Z. contributed to DFT calculations. K.H. and P.C. revised the manuscript. All authors have given approval to the final version of the manuscript.

Notes

The authors declare no competing financial interest.

■ ACKNOWLEDGMENTS

This work is financially supported by the National Key R&D Program of China (2022YFB2404800), the NSFC-Henan Joint Funding (No. U2004210), the Shenzhen Science and Technology Program (JCYJ20210324141613032 and JCYJ20230807143612026), and the City University of Hong Kong Donation Research Grants (DON-RMG 9229021 and 9220061). The authors are grateful for the facility support provided by the Analytical and Testing Center of Huazhong University of Science and Technology and Shiyanjia Lab (www.shiyanjia.com).

REFERENCES

(1) Sun, L.; Liu, Y.; Shao, R.; Wu, J.; Jiang, R.; Jin, Z. Recent Progress and Future Perspective on Practical Silicon Anode-Based Lithium Ion Batteries. *Energy Storage Mater.* **2022**, *46*, 482−502.

(2) Wu, F.; Maier, J.; Yu, Y. Guidelines and Trends for Next-Generation Rechargeable Lithium and Lithium-ion Batteries. *Chem. Soc. Rev.* **2020**, *49*, 1569−1614.

(3) Li, J. Y.; Xu, Q.; Li, G.; Yin, Y. X.; Wan, L. J.; Guo, Y. G. Research Progress Regarding Si-Based Anode Materials Towards Practical Application in High Energy Density Li-Ion Batteries. *Mater. Chem. Front.* **2017**, *1*, 1691−1708.

(4) Lee, J. K.; Oh, C.; Kim, N.; Hwang, J. Y.; Sun, Y. K. Rational Design of Silicon-Based Composites for High-Energy Storage Devices. *J. Mater. Chem. A* **2016**, *4*, 5366−5384.

(5) Lee, Y.; Lee, T.; Hong, J.; Sung, J.; Kim, N.; Son, Y.; Ma, J.; Kim, S. Y.; Cho, J. Stress Relief Principle of Micron-Sized Anodes with Large Volume Variation for Practical High-Energy Lithium-Ion Batteries. *Adv. Funct. Mater.* **2020**, *30*, No. 202004841.

(6) Szczech, J. R.; Jin, S. Nanostructured Silicon for High Capacity Lithium Battery Anodes. *Energy Environ. Sci.* **2011**, *4*, 56−72.

(7) Ashuri, M.; He, Q.; Shaw, L. L. Silicon as a Potential Anode Material for Li-Ion Batteries: Where Size, Geometry and Structure Matter. *Nanoscale* **2016**, *8*, 74−103.

(8) Jain, R.; Lakhnot, A. S.; Bhimani, K.; Sharma, S.; Mahajani, V.; Panchal, R. A.; Kamble, M.; Han, F.; Wang, C.; Koratkar, N. Nanostructuring versus Microstructuring in Battery Electrodes. *Nat. Rev. Mater.* **2022**, *7*, 736−746.

(9) Ma, Y.; Ma, J.; Cui, G. Small Things Make Big Deal: Powerful Binders of Lithium Batteries and Post-Lithium Batteries. *Energy Storage Mater.* **2019**, *20*, 146−175.

(10) Zou, F.; Manthiram, A. A Review of the Design of Advanced Binders for High-Performance Batteries. *Adv. Energy Mater.* **2020**, *10*, No. 2002508.

(11) Chen, H.; Ling, M.; Hencz, L.; Ling, H. Y.; Li, G.; Lin, Z.; Liu, G.; Zhang, S. Exploring Chemical, Mechanical, and Electrical Functionalities of Binders for Advanced Energy-Storage devices. *Chem. Rev.* **2018**, *118*, 8936−8982.

(12) Li, S.; Liu, Y. M.; Zhang, Y. C.; Song, Y.; Wang, G. K.; Liu, Y. X.; Wu, Z. G.; Zhong, B. H.; Zhong, Y. J.; Guo, X. D. A Review of Rational Design and Investigation of Binders Applied in Silicon-Based Anodes for Lithium-Ion Batteries. *J. Power Sources* **2021**, *485*, No. 229331.

(13) Miranda, A.; Sarang, K.; Gendensuren, B.; Oh, E. S.; Lutkenhaus, J.; Verduzco, R. Molecular Design Principles for Polymeric Binders in Silicon Anodes. *Mol. Syst. Des. Eng.* **2020**, *5*, 709−724.

(14) Yu, Y.; Zhu, J.; Li, Y.; Xu, Q.; Jiang, Y.; Yang, C.; Shi, L.; Chen, L.; Liu, P.; Zhang, J.; Jiang, M. Mixed Ion-Electron Conductive Binders Coupling Superior Stiffness and Toughness Establish Dual Crosslinking Stable Silicon Anodes. *Chem. Eng. J.* **2024**, *479*, No. 147807.

(15) Yu, Y.; Yang, C.; Jiang, Y.; Shang, Z.; Zhu, J.; Zhang, J.; Jiang, M. Robust Nitrogen/Sulfur Co-Doped Carbon Frameworks as Multifunctional Coating Layer on Si Anodes Toward Superior Lithium Storage. *Adv. Energy Mater.* **2024**, *15*, No. 2403086.

(16) Yu, Y.; Yang, C.; Jiang, Y.; Zhu, J.; Zhang, J.; Jiang, M. Consecutive Covalent Bonds Reconstruct Robust Dual-Interfaces by Carbonized Binder to Enable Conductive-Additive-Free Durable Silicon Anode. *Nano Energy* **2024**, *130*, No. 110108.

(17) Sun, Z.; Zhu, J.; Yang, C.; Xie, Q.; Jiang, Y.; Wang, K.; Jiang, M. N-Type Polyoxadiazole Conductive Polymer Binders Derived High-Performance Silicon Anodes Enabled by Crosslinking Metal Cations. *ACS Appl. Mater. Interfaces* **2023**, *15*, 12946−12956.

(18) Yu, Y.; Yang, C.; Jiang, Y.; Zhu, J.; Zhao, Y.; Liang, S.; Wang, K.; Zhou, Y.; Liu, Y.; Zhang, J.; Jiang, M. Sponge-Like Porous-Conductive Polymer Coating for Ultrastable Silicon Anodes in Lithium-Ion Batteries. *Small* **2023**, *19*, No. 2303779.

(19) Liu, Y.; Tai, Z.; Zhou, T.; Sencadas, V.; Zhang, J.; Zhang, L.; Konstantinov, K.; Guo, Z.; Liu, H. K. An All-Integrated Anode via Interlinked Chemical Bonding Between Double-Shelled-Yolk-Structured Silicon and Binder for Lithium-Ion Batteries. *Adv. Mater.* **2017**, *29*, No. 1703028.

(20) Lestriez, B.; Bahri, S.; Sandu, I.; Roue, L.; Guyomard, D. On the Binding Mechanism of CMC in Si Negative Electrodes for Li-Ion Batteries. *Electrochem. Commun.* **2007**, *9*, 2801−2806.

(21) Martin, T. R.; Pekarek, R. T.; Coyle, J. E.; Schulze, M. C.; Neale, N. R. Understanding Why Poly(Acrylic Acid) Works: Decarbonylation and Cross-Linking Provide an Ionically Conductive Passivation Layer in Silicon Anodes. *J. Mater. Chem. A* **2021**, *9*, 21929−21938.

(22) Magasinski, A.; Zdyrko, B.; Kovalenko, I.; Hertzberg, B.; Burtovyy, R.; Huebner, C. F.; Fuller, T. F.; Luzinov, I.; Yushin, G. Toward Efficient Binders for Li-ion Battery Si-Based Anodes: Polyacrylic Acid. *ACS Appl. Mater. Interfaces* **2010**, *2*, 3004−3010.

(23) Zhang, B.; Liu, D.; Xie, H.; Wang, D.; Hu, C.; Dai, L. In-Situ Construction of Chemically Bonded Conductive Polymeric Network for High-Performance Silicon Microparticle Anodes in Lithium-Ion Batteries. *J. Power Sources* **2022**, *539*, No. 231591.

(24) Magasinski, A.; Zdyrko, B.; Kovalenko, I.; Hertzberg, B.; Burtovyy, R.; Huebner, C. F.; Fuller, T. F.; Luzinov, I.; Yushin, G. Toward Efficient Binders for Li-Ion Battery Si-Based Anodes: Polyacrylic Acid. *ACS Appl. Mater. Interfaces* **2010**, *2*, 3004−3010.

(25) Wang, Y.; Xu, H.; Chen, X.; Jin, H.; Wang, J. Novel Constructive Self-Healing Binder for Silicon Anodes with High Mass Loading in Lithium-Ion Batteries. *Energy Storage Mater.* **2021**, *38*, 121−129.

(26) Tong, Y.; Jin, S.; Xu, H.; Li, J.; Kong, Z.; Jin, H.; Xu, H. An Energy Dissipative Binder for Self-Tuning Silicon Anodes in Lithium-Ion Batteries. *Adv. Sci.* **2023**, *10*, No. e2205443.

(27) Zheng, Z.; Gao, H.; Ke, C.; Li, M.; Cheng, Y.; Peng, D. L.; Zhang, Q.; Wang, M. S. Constructing Robust Cross-Linked Binder Networks for Silicon Anodes with Improved Lithium Storage Performance. *ACS Appl. Mater. Interfaces* **2021**, *13*, 53818−53828.

(28) Malik, Y. T.; Shin, S. Y.; Jang, J. I.; Kim, H. M.; Cho, S.; Do, Y. R.; Jeon, J. W. Self-Repairable Silicon Anodes Using a Multifunctional Binder for High-Performance Lithium-Ion Batteries. *Small* **2023**, *19*, No. e2206141.

(29) Hu, Z.; Zhao, R.; Yang, J.; Wu, C.; Bai, Y. Binders for Si Based Electrodes: Current Status, Modification Strategies and Perspective. *Energy Storage Mater.* **2023**, *59*, No. 102776.

(30) Wang, H.; Wu, B.; Wu, X.; Zhuang, Q.; Liu, T.; Pan, Y.; Shi, G.; Yi, H.; Xu, P.; Xiong, Z.; Chou, S. L.; Wang, B. Key Factors for Binders to Enhance the Electrochemical Performance of Silicon Anodes Through Molecular Design. *Small* **2022**, *18*, No. e2101680.

(31) He, Q.; Ning, J.; Chen, H.; Jiang, Z.; Wang, J.; Chen, D.; Zhao, C.; Liu, Z.; Perepichka, I. F.; Meng, H.; Huang, W. Achievements, Challenges, and Perspectives in the Design of Polymer Binders for Advanced Lithium-Ion Batteries. *Chem. Soc. Rev.* **2024**, *53*, 7091−7157.

(32) Yoo, G.; Kim, S.; Chanthad, C.; Cho, M.; Lee, Y. Elastic Rubber-Containing Multifunctional Binder for Advanced Li-S Batteries. *Chem. Eng. J.* **2021**, *405*, No. 126628.

(33) Kang, T.; Chen, J.; Cui, Y.; Wang, Z.; Xu, H.; Ma, Z.; Zuo, X.; Xiao, X.; Nan, J. Three-Dimensional Rigidity-Reinforced SiO(x) Anodes with Stabilized Performance Using an Aqueous Multi-component Binder Technology. *ACS Appl. Mater. Interfaces* **2019**, *11*, 26038−26046.

(34) Zheng, M.; Cai, X.; Tan, Y.; Wang, W.; Wang, D.; Fei, H.; Saha, P.; Wang, G. A High-Resilience and Conductive Composite Binder for Lithium-Sulfur Batteries. *Chem. Eng. J.* **2020**, *389*, No. 124404.

(35) Huang, Q.; Song, J.; Gao, Y.; Wang, D.; Liu, S.; Peng, S.; Usher, C.; Goliaszewski, A.; Wang, D. Supremely Elastic Gel Polymer Electrolyte Enables a Reliable Electrode Structure for Silicon-Based Anodes. *Nat. Commun.* **2019**, *10*, No. 5586.

(36) Wu, S.; Yang, Y.; Liu, C.; Liu, T.; Zhang, Y.; Zhang, B.; Luo, D.; Pan, F.; Lin, Z. In-Situ Polymerized Binder: A Three-in-One Design Strategy for All-Integrated SiO_x Snode with High Mass Loading in Lithium Ion Batteries. *ACS Energy Lett.* **2021**, *6*, 290−297.

https://doi.org/10.1021/acsami.4c22696
ACS Appl. Mater. Interfaces 2025, 17, 21206−21214

(37) Zhao, J.; Jing, J.; Li, W.; Chen, W.; Chen, T.; Zhong, H.; Wang, Y.; Fu, J. Noncovalent Crosslinked Liquid Metal-Incorporated Polymer Binder Based on Multiple Dynamic Bonds for Silicon Microparticle Anode. *Energy Storage Mater.* **2023**, *63*, No. 102991.
(38) Zhang, S.; Liu, K.; Xie, J.; Xu, X.; Tu, J.; Chen, W.; Chen, F.; Zhu, T.; Zhao, X. An Elastic Cross-Linked Binder for Silicon Anodes in Lithium-Ion Batteries with a High Mass Loading. *ACS Appl. Mater. Interfaces* **2023**, *15*, 6594−6602.
(39) Oh, J.; Choi, S. H.; Chang, B.; Lee, J.; Lee, T.; Lee, N.; Kim, H.; Kim, Y.; Im, G.; Lee, S.; Choi, J. W. Elastic Binder for High-Performance Sulfide-Based All-Solid-State Batteries. *ACS Energy Lett.* **2022**, *7*, 1374−1382.
(40) Li, G.; Lu, F.; Dou, X.; Wang, X.; Luo, D.; Sun, H.; Yu, A.; Chen, Z. Polysulfide Regulation by the Zwitterionic Barrier Toward Durable Lithium-Sulfur Batteries. *J. Am. Chem. Soc.* **2020**, *142*, 3583−3592.
(41) Kim, J. H.; Lee, K. M.; Kim, J. W.; Kweon, S. H.; Moon, H. S.; Yim, T.; Kwak, S. K.; Lee, S. Y. Regulating Electrostatic Phenomena by Cationic Polymer Binder for Scalable High-Areal-Capacity Li Battery Electrodes. *Nat. Commun.* **2023**, *14*, No. 5721.
(42) Zhang, B.; Dong, Y.; Han, J.; Zhen, Y.; Hu, C.; Liu, D. Physicochemical Dual Cross-Linking Conductive Polymeric Networks Combining High Strength and High Toughness Enable Stable Operation of Silicon Microparticle Anodes. *Adv. Mater.* **2023**, *35*, No. 2301320.
(43) Jeong, D.; Yook, J.; Kwon, D. S.; Shim, J.; Lee, J. C. Interweaving Elastic and Hydrogen Bond-Forming Polymers into Highly Tough and Dtress-Relaxable Binders for High-Performance Silicon Anode in Lithium-Ion Batteries. *Adv. Sci.* **2023**, *10*, No. 2302027.
(44) Lin, X.; Wen, Y.; Wang, J.; Shang, H.; Liu, H.; Xu, X. Boston Ivy-Inspired Natural-Rich Binder with Strong Adhesion for Advanced Silicon-Based Anodes. *Chem. Eng. J.* **2023**, *468*, No. 143784.
(45) Lin, X.; Yu, L.; Wen, Y.; Qi, L.; Wang, S.; Liu, H.; Xu, X.; Chen, C. Tunicate-Inspired Versatile Binder for Silicon/Graphite Anodes Enabled by Co-Operation of π-π Stacking and Hydrogen Bonding Interactions. *Cell Rep. Phys. Sci.* **2023**, *4*, No. 101730.
(46) Hu, K.; Chen, J.; Zhang, J.; Sang, X.; Meng, T.; Wang, Z.; Hu, X. Binder-Enabled Cross-Scale Stabilization of High-Areal-Capacity Micro-Sized Silicon Anodes for High-Voltage Lithium-Ion Batteries. *Energy Storage Mater.* **2025**, *75*, No. 104029.
(47) Hu, L.; Zhang, X.; Zhao, P.; Fan, H.; Zhang, Z.; Deng, J.; Ungar, G.; Song, J. Gradient H-Bonding Binder Enables Stable High-Areal-Capacity Si-Based Anodes in Pouch Cells. *Adv. Mater.* **2021**, *33*, No. 2104416.
(48) Cui, Z.; Gao, F.; Cui, Z.; Qu, J. A second nearest-neighbor embedded atom method interatomic potential for Li−Si alloys. *J. Power Sources* **2012**, *207*, 150−159.

https://doi.org/10.1021/acsami.4c22696
ACS Appl. Mater. Interfaces 2025, 17, 21206−21214

Supporting Information

High-Toughness and Hierarchical Stress-Dissipating Binder Based on Physicochemical Dual-Crosslinking for High-Performance Silicon Anodes

Yang He [a, ‡], *Feng Zhou* [a, ‡], *Yingxi Zhang* [a, b], *Tuan Lv* [a], *Paul K. Chu* [b], *Kaifu Huo* [a,*]

[a] Wuhan National Laboratory for Optoelectronics (WNLO), Huazhong University of Science and Technology, Wuhan, 430074, P. R. China

E-mail: kfhuo@hust.edu.cn (K. F. Huo)

[b] Department of Physics, Department of Materials Science and Engineering, and Department of Biomedical Engineering, City University of Hong Kong, Tat Chee Avenue, Kowloon, Hong Kong 999077, China

[‡] Yang He and Feng Zhou contributed equally to this work

Characterization

Tensile strength and 180^{o} peeling tests

The shear viscosity is determined on the HAAKE MARS60, and the stress-strain and 180^{o} peeling tests are performed on an automatic tensile tester (PARAM). In the tensile strength test in the dry state, the binder membranes are cut into strips of 1 cm × 4 cm and tested at a stretching speed of 25 mm min^{-1}. The tensile strength tests are carried out in the wet state by immersing the samples in the liquid electrolyte for 100 h before testing. For dynamic mechanical tests, tensile tests are repeated 5 times for each sample. In the 180^{o} peeling tests, the Si electrodes are cut into strips of 2.5 cm × 4 cm, and the samples are peeled at a speed of 5 cm min^{-1}.

Linear sweep voltammetry (LSV) and cyclic voltammetry (CV)

In the LSV test, the PAA, LPU-PAA, and CPU-PAA binder membranes are the separators, and steel and lithium are the counter electrodes. The coin cells assembled are tested in the voltage range of 0 to 5 V. In the CV test, Si//Li half-cells are assembled and assessed in the voltage range of 0.01 to 2.0 V at a scanning rate of 0.1 mV s^{-1}, and Cu//Li half-cells are assembled and assessed in the voltage range of 0.01 to 1.5 V at a scanning rate of 0.2 mV s^{-1}.

Rate and cycle testing

The half-cells are charged/discharged at 0.01-1.0 V, with each cell containing 60 μL of the liquid electrolyte (1M $LiPF_6$ in EC: DEC = 1:1 vol % with 10% FEC and 1% VC). With

regard to the full cells, the cathodes and anodes are NCM and Si, respectively, and the N/P ratio is 1.0-1.05. The full cells are charged/discharged at 2.7-4.3 V.

Finite Element Analysis

The finite element analysis (FEA) is conducted using the COMSOL software using the electrochemical and solid mechanics mode. A 3D geometric model is constructed to cater to the specifics of the battery system and electrode configuration. The microscale geometry 3D microstructure is reconstructed based on the nanoscale X-ray computed tomography data.[1] The upper surface of the model is a Li foil which is the counter electrode supplying Li^+. The separation between electrodes is established to emulate the diaphragm thickness. The linear elastic material model is adopted to simulate the stress field caused by lithiation. The solution in the electrochemical model is used to calculate the stress and deformation of the binder and silicon particles. As the lithium concentration increased in the silicon electrode, the materials expanded. The expansion is defined as a function of the local solid lithium concentration (also considered as SOC) derived from our experimental data (Figure S21a) and Cui's theoretical work (mechanical property versus intercalation level for Li_xSi, Figure S21b).[2] The key parameters input into the model are listed in Table S4.

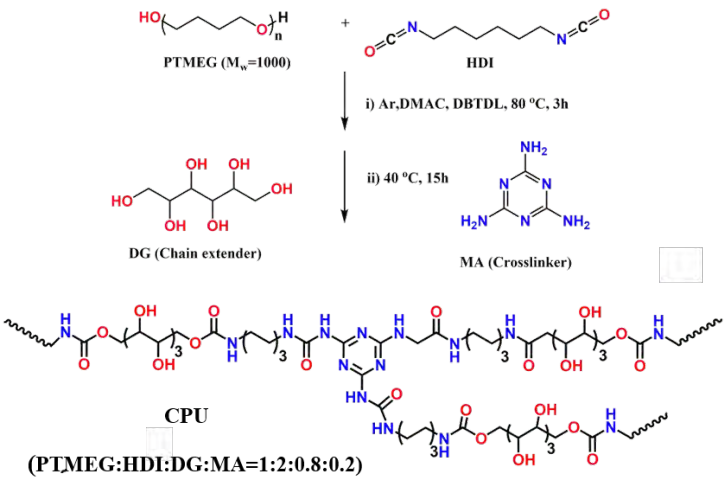

Figure S1. Synthesis and chemical structure of CPU.

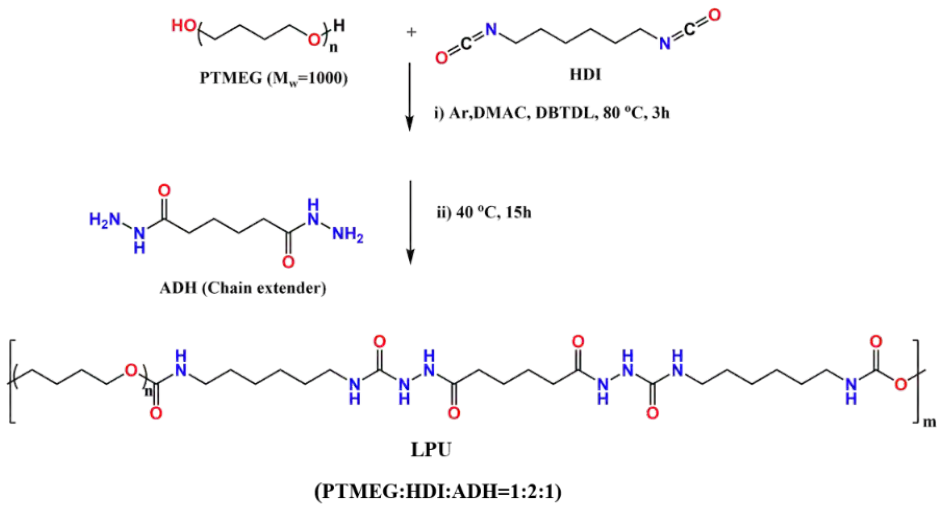

Figure S2. Synthesis and chemical structure of LPU.

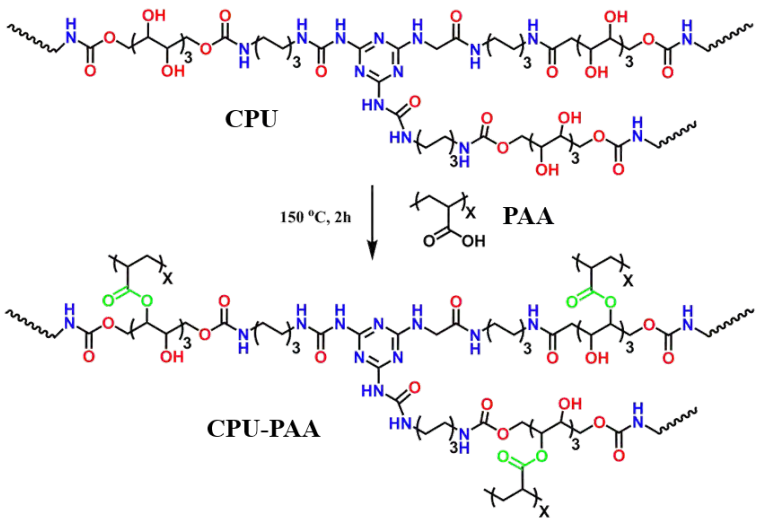

Figure S3. Synthesis and chemical structure of CPU-PAA.

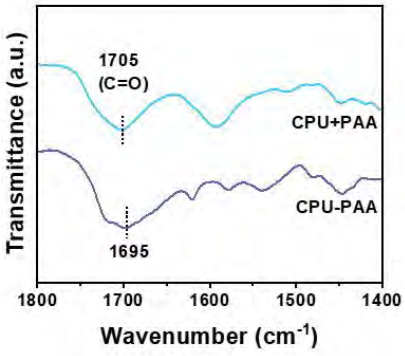

Figure S4. ATR-FTIR spectra of CPU+PAA and CPU-PAA.

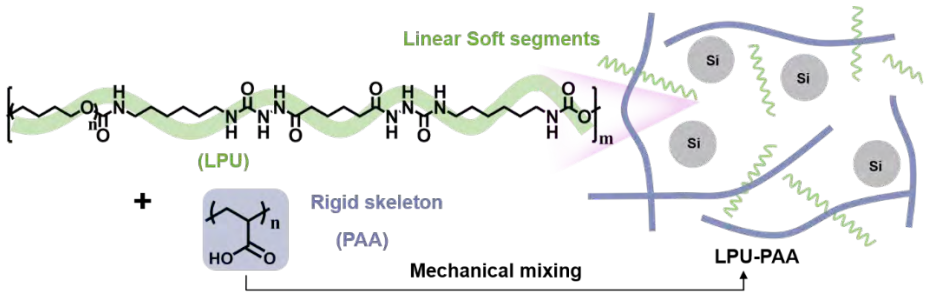

Figure S5. Chemical structure of LPU-PAA.

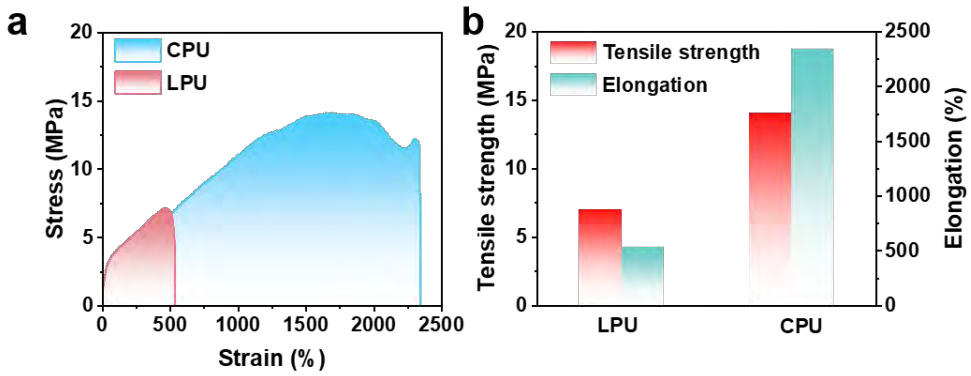

Figure S6. Mechanical properties of LPU and CPU: (a) Stress-strain curves of LPU and CPU and (b) Tensile strength and elongation of LPU and CPU.

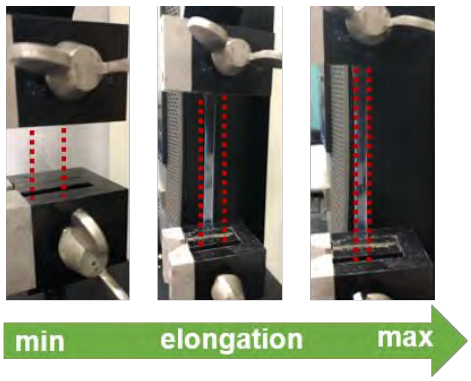

Figure S7. Pictures of the CPU-PAA binder during the stretching test after immersion in the liquid electrolyte for 100 h.

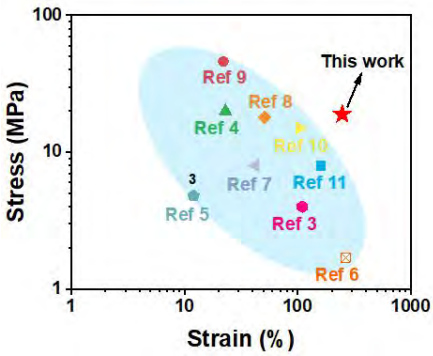

Figure S8. Comparison of the stress and strain of the CPU-PAA binder and thost of similar binders in the literature.[3-11]

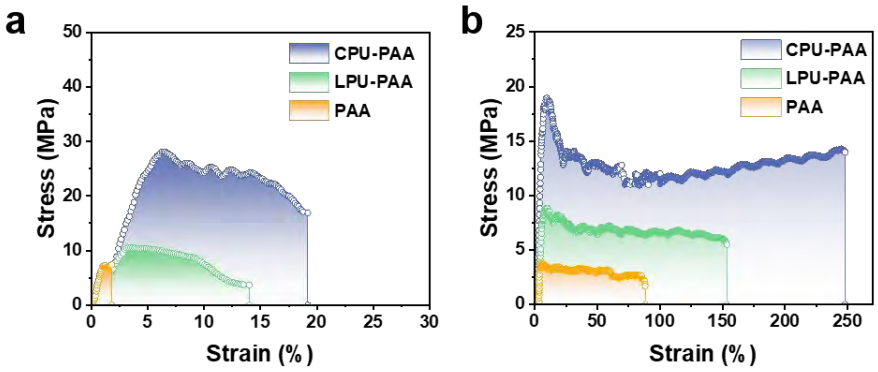

Figure S9. Stress-strain curves of the PAA, LPU-PAA, and CPU-PAA: (a) Dry state and (b) Wet state.

Figure S10. Optical photographs of (a-c) PAA, (d-f) CPU, and (g-i) CPU-PAA polymer films in the initial, folded, and twisted states, optical photographs of the (j) thickness, (k) mass, and (l) load-bearing capacity of the CPU-PAA film.

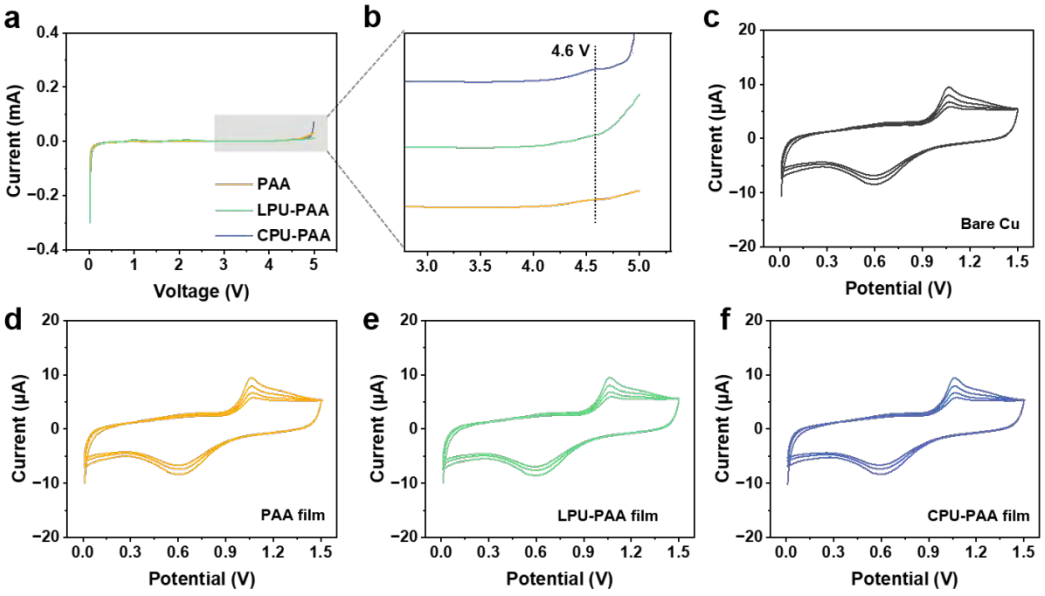

Figure S11. (a-b) LSV curves of PAA, LPU-PAA, and CPU-PAA. CV profiles of (c) bare Cu foil, (d) Cu foil with PAA, (e) Cu foil with LPU-PAA, and (f) Cu foil with CPU-PAA in Li//Cu cells between 0.01 V and 1.5 V at 0.2 mV s^{-1}.

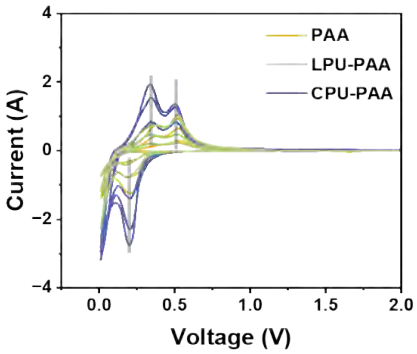

Figure S12. CV curves of Si/PAA//Li, Si/LPU-PAA//Li, and Si/CPU-PAA//Li half-cells.

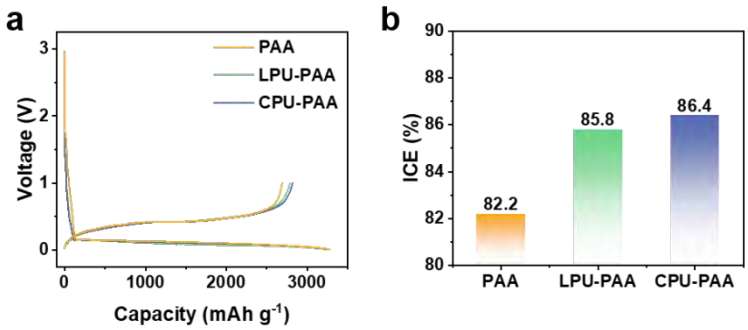

Figure S13. (a) The first voltage-capacity curves of Si electrodes with different binds in Si//Li half cells, and (b) comparison of the initial coulombic efficiency.

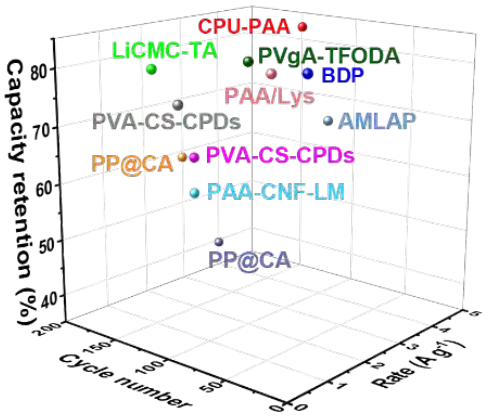

Figure S14. Comparison of the capacity retention of the Si electrode with the CPU-PAA binder with those of similar binders in the literature.[9, 11-17]

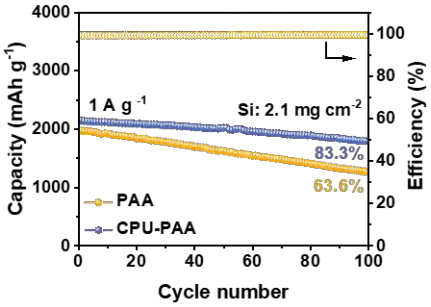

Figure S15. Cycling performance of Si/PAA and Si/CPU-PAA anodes with a Si mass loading of 2.1 mg cm^{-2}.

Figure S16. Pictures of the Si/PAA, Si/LPU-PAA, and Si/CPU-PAA electrodes after 200 cycles at 1 A g^{-1}.

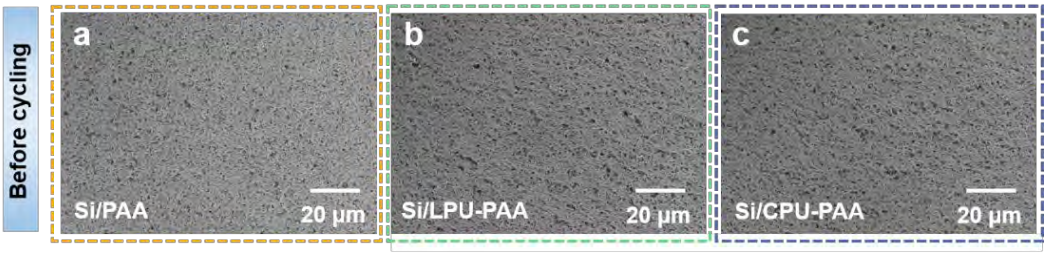

Figure S17. Initial top-view morphology of the (a) Si/PAA, (b)Si/LPU-PAA, and (c) Si/CPU-PAA electrodes.

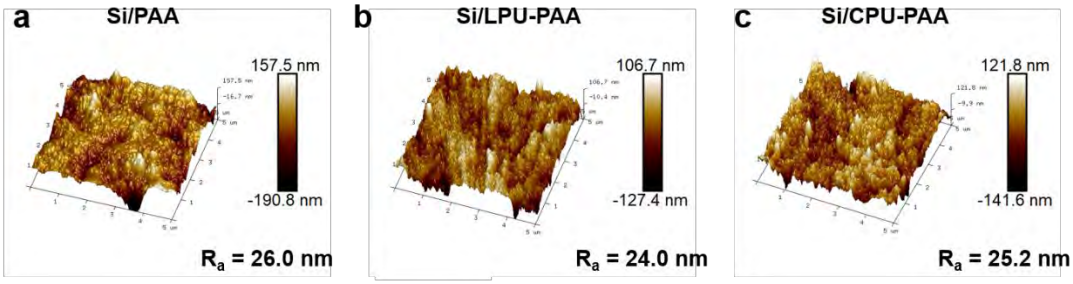

Figure S18. AFM images of the pristine (a) Si/PAA, (b)Si/LPU-PAA, and (c) Si/CPU-PAA electrodes.

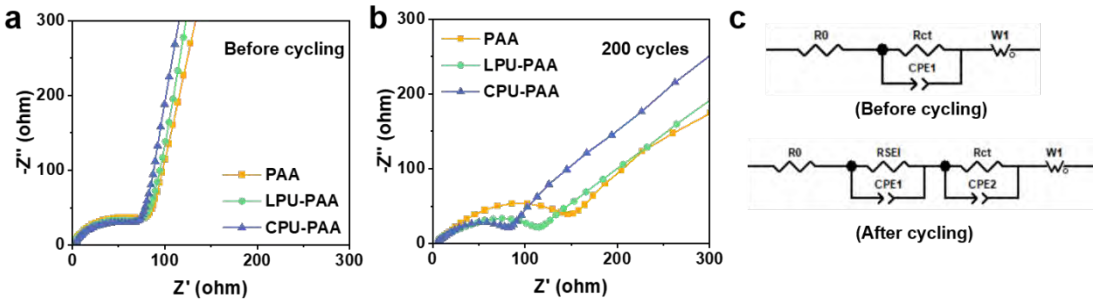

Figure S19. EIS curves of Si electrodes with PAA, LPU-PAA, and CPU-PAA binders (a) before cycling, and (b) after 200 cycles in Si//Li half-cells. (c) The corresponding equivalent circuit before and after cycling fitted by Zview software.

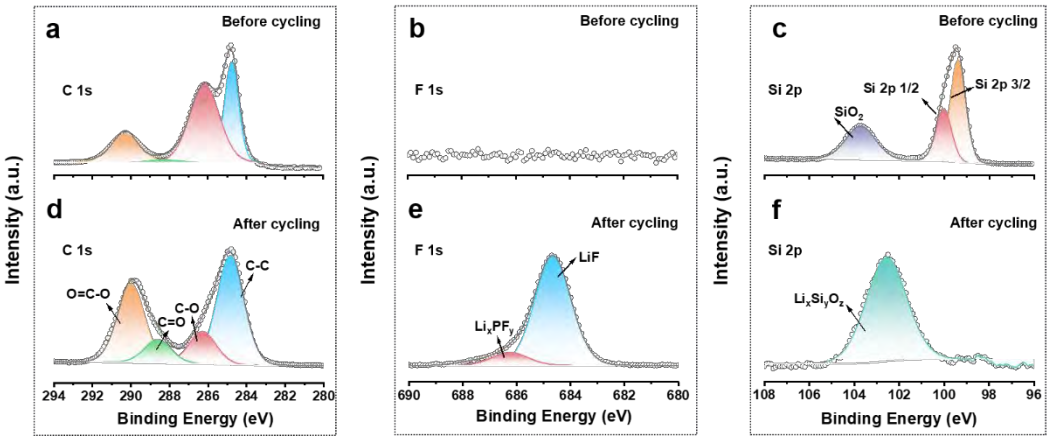

Figure S20. XPS spectra of the Si/CPU-PAA electrode: (a) C 1s, (b) F 1s , and (c) Si 2p before cycling. (d) C 1s, e) F 1s, and (f) Si 2p after cycling.

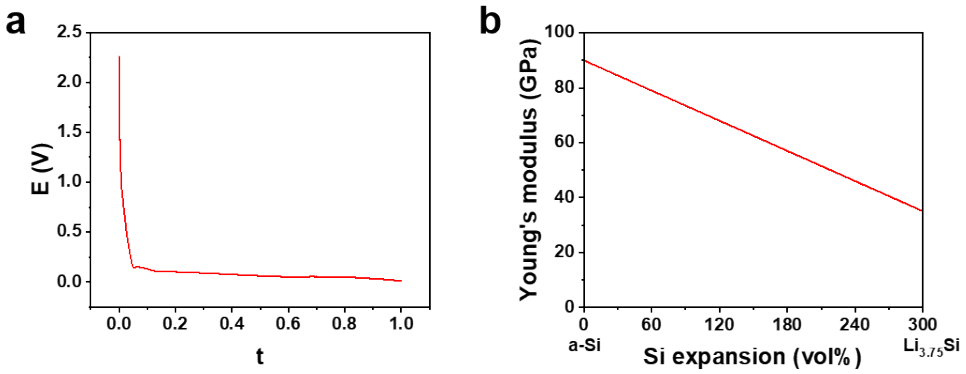

Figure S21. (a) Si 0.1C voltage curve after normalization and (b) Young's modulus of Si as a function of the lithiation state.

Table S1. The GPC data of CPU and LPU.

	M_n (Da)	M_w (Da)	M_p (Da)	M_z (Da)	M_z/M_w
LPU	111904	183318	137598	293270	1.5998
CPU	115162	225641	117758	534786	2.3700

Table S2. Comparison of the tensile strength and toughness of the binders.

Binders	Tensile strength (MPa)	Toughness (MJ m^{-3})
CPU-PAA	18.9	31.5
SSIP[3]	51.6	18.5
xPUU1k[18]	58	4.9
PAA-CNF-LM[11]	8	8.3
Ca-Alg[19]	50	13.5
PAA/EVA[20]	5.67	5.68

Table S3. Comparison of charge transfer resistance of anodes with different binders.

	R_{ct}-pristine (Ω)	R_{ct}-200 cycles (Ω)
CPU-PAA	72.5	85.2
LPU-PAA	78.1	119.4
PAA	79.0	148.3

Table S4. FEA model input parameters.

Parameters	Symbols (unit)	Values
Maximum solid lithium concentration	c_s (mol/m^3)	278 000
Initial electrolyte concentration	c_0 (mol/m^3)	1000
Solid diffusion coefficient	D_s (m^2/s)	1×10^{-12}
Young's modulus of PAA	E_A (GPa)	10.1
Young's modulus of CPU-PAA	E_B (GPa)	7.0
Poisson's ratio	/	0.25

References

1. Ebner, M.; Geldmacher, F.; Marone, F.; Stampanoni, M.; Wood, V. X-Ray Tomography of Porous, Transition Metal Oxide Based Lithium Ion Battery Electrodes. *Adv. Energy Mater.* **2013**, *3*, 845-850.

2. Cui, Z.; Gao, F.; Cui, Z.; Qu, J. A Second Nearest-Neighbor Embedded Atom Method Interatomic Potential for Li-Si Alloys. *J. Power Sources* **2012**, *207*, 150-159.

3. Cai, Y.; Liu, C.; Yu, Z.; Ma, W.; Jin, Q.; Du, R.; Qian, B.; Jin, X.; Wu, H.; Zhang, Q.; Jia, X. Slidable and Highly Ionic Conductive Polymer Binder for High-Performance Si Anodes in Lithium-Ion Batteries. *Adv. Sci.* **2022,** *10*, e2205590.

4. Deng, L.; Deng, S. S.; Pan, S. Y.; Wu, Z. Y.; Hu, Y. Y.; Li, K.; Zhou, Y.; Li, J. T.; Huang, L.; Sun, S. G. Multivalent Amide-Hydrogen-Bond Supramolecular Binder Enhances the Cyclic Stability of Silicon-Based Anodes for Lithium-Ion Batteries. *ACS Appl Mater Interfaces* **2021**, *13*, 22567-22576.

5. Li, M.; Zhang, J.; Gao, Y.; Wang, X.; Zhang, Y.; Zhang, S. A Water-Soluble, Adhesive and 3D Cross-Linked Polyelectrolyte Binder for High-Performance Lithium-Sulfur Batteries. *J. Mater. Chem. A* **2021**, *9*, 2375-2384.

6. Liu, Z.; Fang, C.; He, X.; Zhao, Y.; Xu, H.; Lei, J.; Liu, G. In Situ-Formed Novel Elastic Network Binder for a Silicon Anode in Lithium-Ion Batteries. *ACS Appl Mater Interfaces* **2021**, *13*, 46518-46525.

7. Liu, Z. K.; Deng, S. S.; Zhou, Y.; Tong, Z.; Liu, J. K.; Wang, Z.; Guo, M. J.; Deng,

L.; Zhen, Y.; Li, J. T.; Xu, J. M.; Sun, S. G. On-Site Cross-Linking of Polyacrylamide to Efficiently Bind the Silicon Anode of Lithium-Ion Batteries. *ACS Appl Mater Interfaces* **2023**, *15*, 24416-24426.

8. Ren, W. F.; Le, J. B.; Li, J. T.; Hu, Y. Y.; Pan, S. Y.; Deng, L.; Zhou, Y.; Huang, L.; Sun, S. G. Improving the Electrochemical Property of Silicon Anodes through Hydrogen-Bonding Cross-Linked Thiourea-Based Polymeric Binders. *ACS Appl Mater Interfaces* **2021**, *13*, 639-649.

9. Tang, B.; He, S.; Deng, Y.; Shan, Y.; Qin, H.; Noor, H.; Hou, X. Advanced Binder with Ultralow-Content for High Performance Silicon Anode. *J. Power Sources* **2023**, *556*, 232237.

10. Hu, L.; Zhang, X.; Zhao, P.; Fan, H.; Zhang, Z.; Deng, J.; Ungar, G.; Song, J. Gradient H-Bonding Binder Enables Stable High-Areal-Capacity Si-Based Anodes in Pouch Cells. *Adv. Mater.* **2021**, *33*, 2104416.

11. Zhao, J.; Jing, J.; Li, W.; Chen, W.; Chen, T.; Zhong, H.; Wang, Y.; Fu, J. Noncovalent Crosslinked Liquid Metal-Incorporated Polymer Binder Based on Multiple Dynamic Bonds for Silicon Microparticle Anode. *Energy Storage Mater.* **2023**, *63*, 102991.

12. Zhang, J.; Yan, L.; Zhao, Y.; Su, Y.; Sun, J.; Jiang, H.; Ma, T. A Multifunctional Supramolecular Polymer Binder with Hard/Soft Phase Interaction for Si-Based Lithium-Ion Batteries. *Nano Energy* **2024**, *125*, 109573.

13. Zhang, S.; Liu, K.; Xie, J.; Xu, X.; Tu, J.; Chen, W.; Chen, F.; Zhu, T.; Zhao, X. An

Elastic Cross-Linked Binder for Silicon Anodes in Lithium-Ion Batteries with a High Mass Loading. *ACS Appl Mater Interfaces* **2023**, *15*, 6594-6602.

14. Wu, Z.; Wan, Z.; Li, Z.; Du, Q.; Wu, T.; Cao, J.; Ling, M.; Liang, C.; Tan, Y. Partially Carbonized Polymer Binder with Polymer Dots for Silicon Anodes in Lithium-Ion Batteries. *Small* **2023**, *19*, e2205065.

15. Chen, B.; Xu, D.; Chai, S.; Chang, Z.; Pan, A. Enhanced Silicon Anodes with Robust SEI Formation Enabled by Functional Conductive Binder. *Adv. Funct. Mater.* **2024**, *34*, 2401794.

16. Kwon, O.; Kim, T. Y.; Kim, T.; Kang, J.; Jang, S.; Eom, H.; Choi, S.; Shin, J.; Park, J.; Seol, M. L.; Han, J. W.; Park, S.; Lee, H. W.; Nam, I. Intelligent Stress-Adaptive Binder Enabled by Shear-Thickening Property for Silicon Electrodes of Lithium-Ion Batteries. *Adv. Energy Mater.* **2024**, *14*, 2304085.

17. Nam, S.; Kim, Y.; Kim, S. H.; Son, H. B.; Han, D. Y.; Kim, Y. H.; Cho, J. H.; Park, J.; Park, S. Tailoring Three-Dimensional Cross-Linked Networks Based on Water-Soluble Polymeric Materials for Stable Silicon Anode. *ACS Appl. Mater. Interfaces* **2023**, *16*, 594-604.

18. Jeong, D.; Yook, J.; Kwon, D. S.; Shim, J.; Lee, J. C. Interweaving Elastic and Hydrogen Bond-Forming Polymers into Highly Tough and Stress-Relaxable Binders for High-Performance Silicon Anode in Lithium-Ion Batteries. *Adv. Sci.* **2023**, *10*, 2302027.

19. Yoon, J.; Oh, D. X.; Jo, C.; Lee, J.; Hwang, D. S. Improvement of Desolvation and

Resilience of Alginate Binders for Si-Based Anodes in a Lithium Ion Battery by Calcium-Mediated Cross-Linking. *Phys. Chem. Chem. Phys.* **2014**, *16*, 25628-25635.

20. Guo, R.; Zhang, S.; Ying, H.; Yang, W.; Wang, J.; Han, W. Q. New, Effective, and Low-Cost Dual-Functional Binder for Porous Silicon Anodes in Lithium-Ion Batteries. *ACS Appl Mater Interfaces* **2019**, *11*, 14051-14058.